Integrated single grating compressor for variable pulse front tilt in simultaneously spatially and temporally focused systems

Erica Block,[1,*] Jens Thomas,[1,2] Charles Durfee,[1] and Jeff Squier[1]

[1]*Department of Physics, Colorado School of Mines, 1523 Illinois Street, Golden, Colorado 80401, USA*

[2]*Institute of Applied Physics, Abbe Center of Photonics, Friedrich-Schiller-Universitt Jena, Max-Wien-Platz 1, 07743 Jena, Germany*

Corresponding author: eblock@mines.edu

A Ti:Al$_3$O$_2$ multipass chirped pulse amplification system is outfitted with a single-grating, simultaneous spatial and temporal focusing (SSTF) compressor platform. For the first time, this novel design has the ability to easily vary the beam aspect ratio of an SSTF beam, and thus the degree of pulse-front tilt at focus, while maintaining a net zero-dispersion system. Accessible variation of pulse front tilt gives full spatiotemporal control over the intensity distribution at the focus and could lead to better understanding of effects such as nonreciprocal writing and SSTF-material interactions.   © 2014 Optical Society of America

OCIS codes: (190.7110) Ultrafast nonlinear optics; (320.5520) Pulse compression; (320.7100) Ultrafast measurements.
http://dx.doi.org/10.1364/OL.39.006915

The utility of simultaneous spatiotemporal focusing (SSTF) [1,2] is gaining enthusiasm and has begun to be exploited in the field of microfluidic devices [3] and micromachining [4,5] for its ability to support large focal volumes and long working distances while mitigating nonlinear effects. Additionally, the highly localized nature of an SSTF beams' axial intensity has proved to be an optimal tool for precision tasks such as (1) the ablation of ocular tissue [6] and localized breakdown in water [7] with low numerical aperture beams and (2) the minimization of out-of-focus background excitation in nonlinear microscopy [8,9]. A direct result of the SSTF scheme is intrinsic pulse-front tilt (PFT), a phenomenon where the arrival time of a pulse varies across the beam at focus due to spatial chirp. Optical elements inducing angular dispersion, such as a diffraction grating or prism, will result in PFT. It has been experimentally shown that PFT offers yet another degree of freedom for machining in addition to laser parameters (such as repetition rate, pulse duration, pulse energy, and wavelength), innate material properties, and the numerical aperture (NA) of the beam [10–12]. More specifically, PFT gives rise to nonreciprocal writing, where induced material modifications are dependent on the scan direction relative to the PFT [4,10,13–15].

Tuning PFT in a classical laser machining setup architecture, however, is cumbersome and is not a practical tool for continuous machining. Having the freedom to continuously tune the PFT in a simple manner and in a way that could be automated would broaden the capability and expand the applicability of femtosecond laser micromachining. Additionally, while the use of spatially chirped beams has resulted in intriguing applications as described above, comparison across different groups has been complicated by the number of techniques used to create the spatial chirp (and thereby PFT). In early work, PFT was realized by imposing misalignment within a laser's grating compressor [16]. These misalignments are difficult to quantify because of the number of degrees of freedom involved. Introducing a

grating angular mismatch of the gratings leads to angular spatial chirp, and adjusting the retroreflection mirrors in a double-pass grating pair leads to transverse spatial chirp. A second technique in use is where a single grating is effectively imaged to the target, where the angularly dispersed frequency components cross. This configuration has applications in imaging [1,2], but is not ideal for micromachining because the spatial and temporal focal planes are typically not overlapped. That is, the Gaussian waist of the frequency dispersed beamlets and the location where the beamlets cross may not occur at the same point. In our previous work, we demonstrated that SSTF could provide precise control over PFT by using a single-pass grating compressor configuration [4–6]. This setup, however, is inefficient and unnecessarily convoluted since a secondary SSTF grating compressor is added in conjunction with a complete chirped pulse amplification (CPA) system.

Recently, we addressed this by demonstrating an integrated SSTF platform in a high average power Yb:CaF$_2$ femtosecond amplifier [17], improving the overall efficiency of the SSTF framework and reducing its complexity. Here, we expand upon this idea to create a innovative single grating, integrated SSTF system that in addition allows for smooth variation of PFT for the first time.

In this configuration, the PFT results from the geometry of the gratings and the focusing optic, so it can be precisely controlled, and can be routinely achieved across different systems while maintaining a spatially diffraction-limited and temporally transform-limited focus. Since the beamlets (each frequency component can be treated as its own Gaussian beamlet) are collimated and parallel to each other, there is no transverse chirp at the focal plane. This leads to a coincidence of the temporal and spatial focus. The pulse front tilt results from the angular spatial chirp rate. Following the notation in our previous work [18], let the transverse shift of a beamlet at frequency ω at the entrance of the lens be $\alpha(\omega - \omega_o)$, where ω_o is the central frequency and α is a parameter that describes the spatial chirp rate, whose

beamlet is traveling along the optical axis ($x = 0$). When focused by the lens, of focal length f, the spatial phase is then given by

$$\phi(x, \omega) = -\frac{\omega}{c}\frac{\alpha}{f}(\omega - \omega_o)x. \quad (1)$$

Here, the negative sign comes from the convention that forward-propagating (toward larger z) positive beam angles travel from $-x$ to $+x$. The tilt in the pulse front is the variation of the group delay across the focal plane:

$$\text{PFT} = \frac{\partial \tau_g}{\partial x} = \frac{\partial}{\partial x}\left(\frac{\partial \phi}{\partial \omega}\bigg|_{\omega = \omega_o}\right) = -\frac{\alpha}{f}\frac{\omega_o}{c}. \quad (2)$$

The PFT can be represented in two alternative forms that help connect it to what can be observed in the lab. Let $\Delta\omega$ be the $1/e^2$ intensity half width of the spectrum, and $\tau = 2/\Delta\omega$ be the corresponding half-width pulse duration. (Note that the corresponding full width at half-maximum is $\tau_{\text{fwhm}} = \tau\sqrt{2\ln 2}$). Then the numerical aperture of the focusing in the spatial chirp direction is

$$\text{NA}_{\text{sc}} = \sin\theta_x \approx \frac{\alpha\Delta\omega}{f}. \quad (3)$$

We can now make use of this to reformulate the PFT as

$$\text{PFT} = -\frac{\pi\tau}{\lambda_0}\text{NA}_{\text{sc}}. \quad (4)$$

For a given laser system operating at a central wavelength λ_0 with a transform-limited pulse duration τ, the PFT depends primarily on the angular spread of the spectrum at the focal plane. Another formulation that illustrates the structure of the tilted pulse front is to make use of the spatial chirp rate $\beta = \alpha\Delta\omega/w_{\text{in}}$, where w_{in} is the $1/e^2$ intensity radius of the input Gaussian beamlet. Note that β has a sign that depends on the orientation of the spectrum relative to the x-axis. This ultimately determines the orientation of the tilted pulse front. The PFT can then be described as

$$\text{PFT} = \frac{-\beta\tau}{w_0}, \quad (5)$$

where w_0 is the $1/e^2$ intensity radius of the focal spot. Equation (5) makes it clear that the time taken for the tilted pulse front to cross the full diameter of the beam is $2\beta\tau$.

Our design incorporates our SSTF compressor within a multipass, Ti:Al$_3$O$_2$ CPA system. In this case, the SSTF compressor doubles as the compressor for the CPA system (a one-step process). It consists of a single, 130×20 mm clear aperture, $G = 1200$ lines/mm transmission grating (LightSmyth Technologies). The grating has a throughput of 96% at 800 nm and is situated at an incident angle of $\theta_i = 31.6$ deg to compensate for third-order dispersion. After the grating, two right-angle dihedrals are mounted on carriages atop a precision dovetail optical rail (Newport PRL-36) along the grating's diffracted angle ($\theta_D = 25.9$ deg). Completing the design is a right angle roof mirror that retroreflects the beam back through

the system at a lower height (a double-pass arrangement). The two dihedrals on the rail are mounted at different heights so that upon the first pass through the compressor, the diffracted beam proceeds over the closest dihedral and onto the furthest dihedral (D1). The beam is then redirected through the grating and onto a retroreflecting roof mirror that once again reflects the beam back through the grating but this time at a different (≈ 7 mm lower) height. At this new height, the beam now reflects off the second dihedral (D2) and back through the grating, exiting the compressor along the input beam path. A pick-off mirror at the new lower height directs the beam to a 1″ effective focal length, 90 deg off-axis parabola (Edmund Optics No. 47-095) and 3-axis specimen scanning stages (Aerotech Inc, ANT130-110-XY/ANT130-060-L-Z). A layout of this system is shown in Fig. 1.

The innovation of the design lies in the decoupling of the dihedrals (D1 and D2). Adjusting the separation between D1 and D2 along the rail results in variation of the PFT while maintaining the necessary dispersion compensation for the CPA system. The distances, b_1 and b_2 [illustrated in Fig. 2(a)] are defined here as the optical path between the grating and D1 and the grating and D2 respectively. The difference between b_1 and b_2 is adjusted in order to produce the desired PFT, given by the spectral spread induced by passing through a Treacy grating pair [19,20]:

$$b_1 - b_2 = f\frac{c}{\lambda_0}\frac{\cos^2\theta_D}{G\cos\theta_i}\text{PFT}, \quad (6)$$

That is, PFT arises if $b_1/b_2 \neq 1$. Once the PFT is set, b_2 and b_1 are coupled and translated together to a fixed total
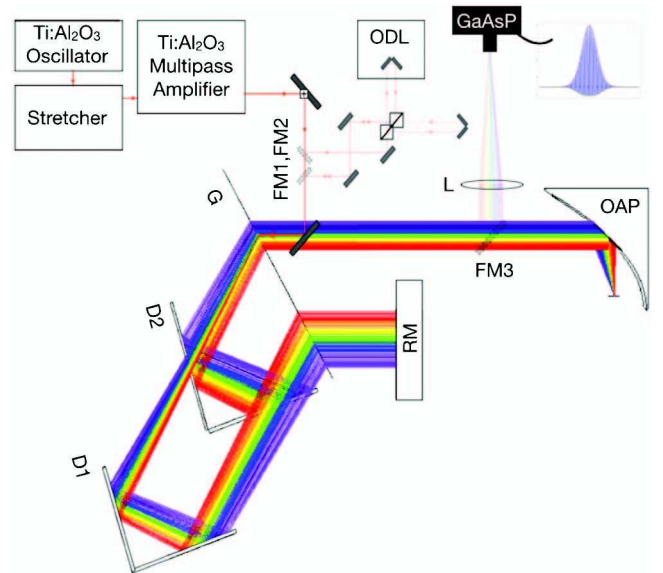

Fig. 1. Schematic of the integrated SSTF system that allows for variable PFT. It consists of a single transmission grating (G), two dihedrals (D1, D2), and a roof mirror (RM). Flip mirrors (FM1, FM2, FM3) before the compressor and off-axis parabola (OAP) redirect the beam through a built-in second-order interferometric autocorrelator and then a lens (L) which focuses the collinear beams onto a GaAsP detector for rapid pulse width measurements. The basic interferometer design incorporates Mesa Photonic's precision Peregrine Optical Delay Line (ODL) in one of the arms.
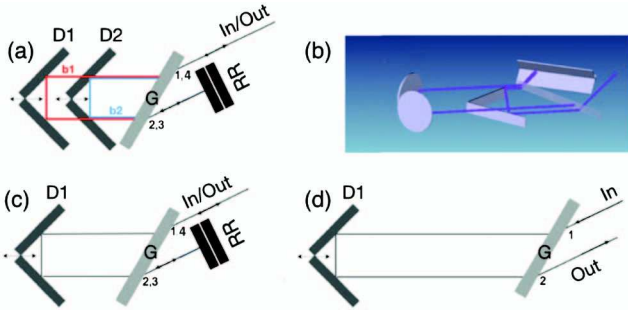
Fig. 2.   Various configurations of dihedrals 1 and 2 (D1, D2) and roof mirror retroreflector (RR) within the variable PFT compressor for the cases of (a,b) variable PFT (c) no-spatial chirp (conventional focus), and (d) maximum PFT.

length needed to compensate for the overall second order dispersion, Φ_2, of the complete system (post amplifier):

$$b_1 + b_2 = \frac{2\pi c^2 \cos^2 \theta_D}{\lambda_0^3 G^2} \Phi_2, \qquad (7)$$

where the convention $\theta_D > 0$ is assumed. The third-order dispersion is

$$\Phi_3 = -\frac{3\lambda_0}{2\pi c}\left(1 + mG\lambda_0 \frac{\sin \theta_D}{\cos^2 \theta_D}\right)\Phi_2 \qquad (8)$$

and should also be fully compensated if the grating constant G and diffraction order m of the stretcher matches with the SSTF grating.

Figure 2 shows various configurations of the compressor. For variable PFT, Fig. 2(a), the spacing, b_1 and b_2, of the dihedrals varies depending on the desired PFT. Figure 2(b) better illustrates the beam path in this configuration in three dimensions. Currently the compressor is arranged to provide a beam aspect ratio (β_{BA}: the ratio of the spatially chirped-to-beamlet widths) of 10 (PFT≈58, 700 fs/mm at focus). Note that it could also be arranged for D1 to pass over D2 ($b_1 < b_2$) in which case it would be possible to tune the PFT through zero to the opposite sign. For zero PFT, Fig. 2(c), D2 is removed from the rail while the compressor remains double passed, eliminating spatial chirp and fully compressing the pulse (i.e., a conventional beam). Separate rail carriages for D1 and D2 keep this process straightforward. With appropriate optomechanics, it would be possible for D1 and D2 to stack in the same plane, $b_1 = b_2$, (eliminating the need to remove D2). However, in our setup, we are mechanically limited. For maximum PFT, Fig. 2(d), D2 is again removed from the rail, but this time the compressor is single passed. The roof mirror, similar to D2, is situated on a translation rail and is easily removed from the beam path.

Figure 3 plots PFT as a function of the difference between dihedral positions ($b_1 - b_2$). Our current PFT regime is marked by a black circle on Fig. 3.

Ascertaining SSTF pulse widths is complicated by the fact that the pulse width is varying throughout the focus. Zhu et al. were the first to characterize SSTF pulses with an interferometric second-order autocorrelation using
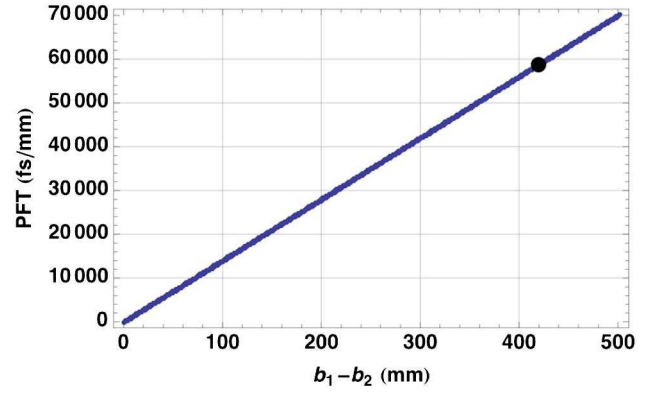

Fig. 3.   PFT as a function of the difference between dihedral positions $(b_1 - b_2)$, Eq. (6). ($f = 25.4$ mm, $G = 1200$ l/mm, $\lambda_0 = 800$ nm, $\theta_D = 25.9$ deg). Our current PFT regime is marked with the black circle.

two-photon excitation fluorescence off a nonlinear element (Rhodamine sample) at focus [2]. Here, we use a similar method for retrieving SSTF pulse widths. We implement Mesa Photonic's interferometrically stable Peregrine Optical Delay Line within a simple interferometer configuration, Fig. 1. The Peregrine has ≈1 cm of travel and a resolution of ≈1 fs. A two-beamsplitter design is used to balance each arm of the interferometer. To measure the pulse width, a flip-up mirror before the compressor redirects the beam through the interferometer setup. The two collinear pulses are then compressed and weakly focused into a large area, 6×6 mm, GaAsP diode using a long focal length ($f = 75$ cm) lens. Focusing is necessary since only at the focus are all the wavelengths overlapped to produce a short pulse. The long focal length lens helps avoid aberrations that spatially chirped beams are susceptible to when focusing through refractive optics, most notably chromatic aberration. Using this method, our SSTF pulse duration was determined to be 85 fs at focus, assuming a Gaussian pulse shape.

Careful attention must be paid to the alignment of the dihedrals within the compressor. Misalignment of a dihedral's vertical tilt for instance results in a skewed beam in the x–y plane, Figs. 4(a) and 4(b). This is manifested as an asymmetric artifact within the pulse autocorrelation, Fig. 4(c). To insure alignment, we look in both the near- and far-field while translating each dihedral along the full distance of the rail. Once the first dihedral is aligned, the stationary dihedral (roof mirror) is easily aligned by looking at the passes through the grating with the unmodelocked oscillator beam. Passes 3,4 should be stacked nicely underneath passes 1,2, on the grating.
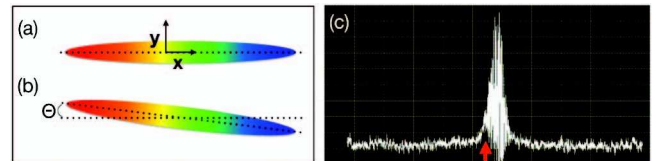

Fig. 4.   (a) Well aligned compressor dihedrals result in a level SSTF beam in the x–y plane. (b) Misaligned compressor dihedrals result in a tilted SSTF beam in the x–y plane. (c) Misalignment of compressor dihedrals is further realized in an autocorrelation trace as overt asymmetry.

In summary we have shown for the first time a novel single grating compressor design that offers the ability to smoothly vary the PFT. This is especially intriguing for micromachining and nonreciprocal writing where PFT provides yet another degree of freedom for material modification based on scan direction. Additionally it may also be of importance for applications requiring no PFT, such as filamentation-based glass-to-glass bonding [21–25]. We can see how the flexibility of this compressor design can now allow for both applications to be realized efficiently with a single system and result in uniquely structured and sealed lab on a chip type devices. Finally, we have also shown that second-order intensity autocorrelations of the SSTF beams can be used to perfect the integrated compressor alignment.

References

1. D. Oron, E. Tal, and Y. Silberberg, Opt. Express **13**, 1468 (2005).
2. G. Zhu, J. van Howe, M. Durst, W. Zipfel, and C. Xu, Opt. Express **13**, 2153 (2005).
3. F. He, H. Xu, Y. Cheng, H. Ni, H. Xiong, Z. Xu, K. Sugioka, and K. Midorikawa, Opt. Lett. **35**, 1106 (2010).
4. D. N. Vitek, E. Block, Y. Bellouard, D. E. Adams, S. Backus, D. Kleinfeld, C. G. Durfee, and J. A. Squier, Opt. Express **18**, 24673 (2010).
5. D. N. Vitek, D. E. Adams, A. Johnson, P. S. Tsai, S. Backus, C. G. Durfee, D. Kleinfeld, and J. A. Squier, Opt. Express **18**, 18086 (2010).
6. E. Block, M. Greco, D. Vitek, O. Masihzadeh, D. A. Ammar, M. Y. Kahook, N. Mandava, C. Durfee, and J. Squier, Biomed. Opt. Exp. **4**, 831 (2013).
7. R. Kammel, R. Ackermann, J. Thomas, J. Götte, S. Skupin, A. Tünnermann, and S. Nolte, Light: Sci. Appl. **3**, e169 (2014).
8. C. Durst, M. E. Zhu, and G. Xu, Opt. Commun. **281**, 1796 (2009).
9. M. E. Durst, G. Zhu, and C. Xu, Opt. Express **14**, 12243 (2006).
10. W. Yang, P. G. Kazansky, Y. Shimotsuma, M. Sakakura, K. Miura, and K. Hirao, Appl. Phys. Lett. **93**, 171109 (2008).
11. J. U. Thomas, E. Block, M. Greco, A. Meier, C. G. Durfee, J. A. Squier, S. Nolte, and A. Tünnermann, Proc. SPIE **8972**, 897219 (2014).
12. B. Sun, P. Salter, and M. Booth, J. Opt. Soc. Am. A **31**, 765 (2014).
13. P. G. Kazansky, W. Yang, E. Bricchi, J. Bovatsek, A. Arai, Y. Shimotsuma, K. Miura, and K. Hirao, Appl. Phys. Lett. **90**, 151120 (2007).
14. B. Poumellec, M. Lancry, J. C. Poulin, and S. Ani-Joseph, Opt. Express **16**, 18354 (2008).
15. P. S. Salter and M. J. Booth, Appl. Phys. Lett. **101**, 141109 (2012).
16. K. Osvay, A. P. Kovacs, Z. Heiner, G. Kurdi, J. Klebniczki, and M. Csatari, IEEE J. Sel. Top. Quantum Electron. **10**, 213 (2004).
17. J. Squier, J. Thomas, E. Block, C. Durfee, and S. Backus, Appl. Phys. A **114**, 209 (2014).
18. C. G. Durfee, M. Greco, E. Block, D. Vitek, and J. A. Squier, Opt. Express **20**, 14244 (2012).
19. A. M. Weiner, *Ultrafast Optics* (Wiley, 2009).
20. E. B. Treacy, IEEE J. Quantum Electron. **5**, 454 (1969).
21. W. Watanabe, S. Onda, T. Tamaki, and K. Itoh, Appl. Phys. B **87**, 85 (2006).
22. T. Tamaki, W. Watanabe, J. Nishii, and K. Itoh, Jpn. J. Appl. Phys. **44**, L687 (2005).
23. T. Tamaki, W. Watanabe, and K. Itoh, Opt. Express **14**, 10460 (2006).
24. W. Watanabe, S. Onda, T. Tamaki, K. Itoh, and J. Nishii, Appl. Phys. Lett. **89**, 20 (2006).
25. K. Sugioka, M. Iida, H. Takai, and K. Micorikawa, Opt. Lett. **36**, 2734 (2011).